

2023-03-28

## CoNi-based Bimetal-organic Framework Derived Carbon Composites Multifunctionally Modified Separators for Lithium-Sulfur Batteries

Yan-Jie Wang

Hong-Yu Cheng

Ji-Yue Hou

Wen-Hao Yang

Rong-Wei Huang

Zhi-Cong Ni

Zi-Yi Zhu

*See next page for additional authors*

---

### Recommended Citation

Yan-Jie Wang, Hong-Yu Cheng, Ji-Yue Hou, Wen-Hao Yang, Rong-Wei Huang, Zhi-Cong Ni, Zi-Yi Zhu, Ying Wang, Ke-Yi Wei, Yi-Yong Zhang, Xue Li. CoNi-based Bimetal-organic Framework Derived Carbon Composites Multifunctionally Modified Separators for Lithium-Sulfur Batteries[J]. *Journal of Electrochemistry*, 2023 , 29(3): 2217002.

DOI: 10.13208/j.electrochem.2217002

Available at: <https://jelectrochem.xmu.edu.cn/journal/vol29/iss3/3>

This Article is brought to you for free and open access by Journal of Electrochemistry. It has been accepted for inclusion in Journal of Electrochemistry by an authorized editor of Journal of Electrochemistry.

---

## CoNi-based Bimetal-organic Framework Derived Carbon Composites Multifunctionally Modified Separators for Lithium-Sulfur Batteries

### Authors

Yan-Jie Wang, Hong-Yu Cheng, Ji-Yue Hou, Wen-Hao Yang, Rong-Wei Huang, Zhi-Cong Ni, Zi-Yi Zhu, Ying Wang, Ke-Yi Wei, Yi-Yong Zhang, and Xue Li

### Corresponding Author(s)

Yi-Yong Zhang(zhangyiyong0918@qq.com);  
Xue Li(438616074@qq.com)

## ARTICLE

# CoNi-based Bimetal-organic Framework Derived Carbon Composites Multifunctionally Modified Separators for Lithium-Sulfur Batteries

Yan-Jie Wang<sup>a,#</sup>, Hong-Yu Cheng<sup>a,#</sup>, Ji-Yue Hou<sup>a</sup>, Wen-Hao Yang<sup>a</sup>,  
Rong-Wei Huang<sup>a</sup>, Zhi-Cong Ni<sup>a</sup>, Zi-Yi Zhu<sup>a</sup>, Ying Wang<sup>a,b</sup>, Ke-Yi Wei<sup>c</sup>,  
Yi-Yong Zhang<sup>a,\*</sup>, Xue Li<sup>a,\*</sup>

<sup>a</sup> National and Local Joint Engineering Laboratory for Lithium-Ion Batteries and Materials Preparation Technology, Key Laboratory of Advanced Battery Materials of Yunnan Province, Faculty of Metallurgical and Energy Engineering, Kunming University of Science and Technology, Kunming 650093, China

<sup>b</sup> College of Intelligent Manufacture, PanZhihua University, Panzhihua 617000, China

<sup>c</sup> Yunnan ZhongYan Industry Co., Ltd. Technology Center, Kunming 650231, China

## Abstract

The commercial application of lithium-sulfur batteries (LSB) is still limited by the irreversible capacity fading caused by the shuttle of lithium polysulfides (LIPS). To address this issue, a bimetal (nickel, cobalt)-organic framework (MOF) derived carbon, (Ni, Co)/C, was prepared to modify the separator. The multifunctionally modified separator effectively captures LIPS, ensuring the stability and reversibility of sulfur fixation, while providing catalytic activity and improving ionic conductivity. The cobalt metal has a larger coordination number, more pore structure distribution, larger specific surface area, more surface C=O, and smaller particle size to achieve a large and rapid chemical sulfur fixation. The high conductivity provided by nickel, and the catalytic activity and the ability to block LIPS shuttling enabled the reversibility of sulfur inhibition. The synergistic effect of cobalt-nickel bimetals significantly improves the cycling stability and rate capability of LSB. At a current density of 1 C, the capacity of the (Ni, Co)/C modified separator battery could reach 1035.6 mAh·g<sup>-1</sup> in the first cycle, the capacity remained at 662.2 mAh·g<sup>-1</sup> after 500 cycles, and the capacity retention rate was 63.9%.

**Keywords:** Lithium-sulfur battery; Modified separator; Bimetal-organic framework derived carbon composites; Shuttle effect

## 1. Introduction

Lithium-sulfur batteries (LSB) have attracted great attention and extensive research by scientists due to the theoretical capacity of sulfur cathodes as high as 1675 mAh·g<sup>-1</sup>, large reserves of sulfur raw materials, and low price. However, many scientific issues such as the dissolution and shuttling of polysulfides in LSB and the corrosion of Li metal anodes still need to be solved urgently. The separator is an important part of LSB. The traditional

polyolefin separator has problems such as poor inhibition of intermediate polysulfides (LIPS) shuttle effect, poor lithium ion migration number and slow conversion kinetics. More and more scholars solve such problems by modifying the separator [1].

In order to realize the physical adsorption and chemical anchoring of polysulfides to alleviate the irreversible capacity fading problem caused by the shuttle effect, some materials rich in pore structures and active sites with surface functional

Received 20 July 2022; Received in revised form 1 August 2022; Accepted 25 October 2022  
Available online 31 October 2022

<sup>#</sup>These authors contributed equally to this work.

\* Corresponding author, Yi-Yong Zhang, Tel: (86)18059238780, E-mail address: zhangyiyong0918@qq.com.

\* Corresponding author, Xue Li, Tel: (86)18213586305, E-mail address: 438616074@qq.com.

<https://doi.org/10.13208/j.electrochem.2217002>

1006-3471/© 2023 Xiamen University and Chinese Chemical Society. This is an open access article under the CC BY 4.0 license (<https://creativecommons.org/licenses/by/4.0/>).

groups are used for separator modifications. Sun et al. [2] used nickel cobaltate/carbon nanofibers ( $\text{NiCo}_2\text{O}_4/\text{CNF}$ ) composites as chemical traps for LIPS. Polar  $\text{NiCo}_2\text{O}_4$  can achieve strong trapping of LIPS by Ni-S and Co-S, and the structurally stable CNF network acts as a second barrier for polysulfides. The  $\text{NiCo}_2\text{O}_4/\text{CNF}$ -based batteries with sulfur loading of  $6.3 \text{ mg}\cdot\text{cm}^{-2}$  can retain a capacity of  $870 \text{ mAh}\cdot\text{g}^{-1}$  after 200 cycles at 0.1 C, with a capacity retention rate as high as 95%. In order to improve the low ion mobility of the separator, the modified layer coated on the conventional separator which faced to the sulfur cathode can be used as a current collector to further accelerate the transfer of electrons to the active material and improve the conductivity of the sulfur cathode, thereby improving the utilization of the active material, such as polymers and carbon materials, etc. [3–6]. Chen et al. [7] used phosphor-doped nickel tellurium ( $\text{P}\text{-NiTe}_{2-x}$ ) immobilized on corn stover carbon (MSC) nanosheets as a separator modification layer for lithium-sulfur batteries ( $\text{MSC}/\text{P}\text{-NiTe}_{2-x}$ ),  $\text{P}\text{-NiTe}_{2-x}$  improves the separator ion mobility well, and the  $\text{MSC}/\text{P}\text{-NiTe}_{2-x}$  modified separator battery achieves ultra-high-capacity retention at high rates. In addition, they [6] also prepared a N-doped carbon nanotube with embedded cobalt nanoparticles (Co-NCNT), and the well-conductive Co-NCNT acts as an internal current collector, enabling fast electron transport. The LSB with the Co-NCNT modified separator at 0.1C with a sulfur loading of  $4.3 \text{ mg}\cdot\text{cm}^{-2}$  still has a high areal capacity of  $3.73 \text{ mAh}\cdot\text{cm}^{-2}$  after 100 cycles. In order to accelerate the conversion kinetics of polysulfides in LSB, modified substances with catalytic activity for sulfur conversion, such as metals and their compounds, are used [8–10]. Chen et al. [11] utilized ultrafine  $\text{CoS}_2$  nanoparticles to catalyze the conversion between  $\text{Li}_2\text{S}_6$  and  $\text{Li}_2\text{S}_2/\text{Li}_2\text{S}$ , thereby improving the redox kinetics of polysulfides. A bifunctional electrocatalytic 1D–2D CoTe MXene modified separator [12] was also developed for LSB. The combination of multiple components and layered structure design accelerated the nucleation and decomposition of  $\text{Li}_2\text{S}$ , and increased the rate performance and cycle stability of LSB.

Although the above studies have made certain contributions in improving ion mobility, alleviating the shuttle effect, and catalyzing sulfur conversion, the modified substances that take into account the three functions are inevitably faced with electrode-scale problems due to their uneven element distribution. Oxidation/reduction reaction heterogeneity [13], which will undoubtedly exacerbate the complexity of the electrochemical

reaction of LSB, and the heterogeneous reaction of polysulfides with the lithium surface will affect the lithium corrosion of the battery [14]. The above problems can be well avoided by using metal-organic frameworks (MOFs) with regular metal frameworks and uniformly distributed metal atoms in LSB. The abundant pore size and large specific surface area of MOFs can physically capture lithium polysulfides in grids [15], and designable metal centers can immobilize sulfur with polysulfide anions through Lewis acid-base interactions, such as Ni, Co and other transition metal centers [16]. In addition, high electrical conductivity can also be obtained by preparing its derivative materials [17–20]. MOFs with different metal centers are used in LSB systems, and their catalytic activities and effects are also different. For example,  $\text{M}_3\text{Mo}_3\text{C}$  ( $\text{M} = \text{Co}, \text{Ni}, \text{Fe}$ ) was used in LSB separator modification, and  $\text{Li}_2\text{S}_8$  could be decomposed into short-chain  $\text{LiS}$ ,  $\text{LiS}_2$  and single S atoms under the catalyses of three metal carbides, among which  $\text{Co}_3\text{Mo}_3\text{C}$  catalytically decomposed the most  $\text{Li}_2\text{S}_8$  has the strongest ability and moderate adsorption capacity for  $\text{Li}_2\text{S}_8$ , so the battery with  $\text{Co}_3\text{Mo}_3\text{C}$  modified separator has better electrochemical performance [21]. Therefore, it is necessary to design multi-component metal-based MOFs for LSB to catalyze the conversion between the numerous LIPS involved in the charge-discharge process through different metal centers. However, due to the different stability constants of coordination between different metals and organic ligands, for example, the stability constants of Cu, Co, Ni complexed with EDTA are 16.6, 14.5, and 17.1, respectively, so the preparation of bimetal-MOFs is challenging. In comparison, bimetal-MOFs have been less studied. The use of bimetal-MOFs in LSB separator modification can specifically catalyze different redox reactions to maximize the electrochemical kinetics and thus enhance the battery performance.

In this work, a columnar nickel-cobalt binary MOF [(Ni,Co)-MOF] was prepared by a simple, low-cost, and highly reproducible room-temperature liquid phase synthesis method. Bimetal-MOF-derived materials [(Ni,Co)/C] are *in situ* generated by high-temperature carbonization for separator modification of LSB. The abundant polar functional groups on the (Ni,Co)/C surface improve the wettability of the electrolyte and realize the chemical anchoring of polysulfides. The metal center exhibits catalytic performance and accelerates the conversion between polysulfides. The porous structure can physically anchor polysulfides and speed up the migration of lithium ions; the higher degree of graphitization provides a

large number of active sites. The mixed distribution of different particle sizes makes it have the advantage of point-to-surface bonding, which is conducive to long-range and short-range, and improve ionic conductivity. Therefore, the improvements in the cycling performance and rate capability of LSB could be achieved by the (Ni,Co)/C modified separator.

## 2. Experimental

### 2.1. Preparation of Ni-MOF-derivative materials

Trimellitic acid was added to a mixed solution of absolute ethanol and deionized water with a volume ratio of 1:1, and the organic ligand solution was obtained after sonication at room temperature for 30 min. 0.73 g of nickel nitrate hexahydrate was added to deionized water, and the nickel ion solution was obtained after sonication at room temperature for 30 min. After the organic ligand solution was stirred uniformly at a speed of 600 rps, the nickel ion solution was poured into it, triethylamine was added rapidly, and the mixture was stirred for 30 min. The solution was suction filtered, washed and dried to obtain Ni-MOF. The obtained Ni-MOF was calcined at 900 °C for 2 h in an argon atmosphere (the heating rate was 5 °C·min<sup>-1</sup>) to obtain the Ni-MOF derived material (Ni/C).

### 2.2. Preparation of Co-MOF-derivative materials

Cobalt nitrate hexahydrate was used as the metal salt, and the rest of the steps were the same as the preparation of Ni-MOF. After carbonization, a Co-MOF derived material (Co/C) was obtained.

### 2.3. Preparation of (Ni, Co)-MOF-derivative materials

0.365 g of cobalt nitrate hexahydrate and 0.365 g of nickel nitrate hexahydrate were dissolved in deionized water to prepare a cobalt-nickel double metal ion solution. The remaining steps were the same as the preparation of Ni-MOF. After carbonization, a (Ni,Co)-MOF derivative material [(Ni,Co)/C] was obtained.

### 2.4. Material characterization

The structures of the as-prepared materials were studied by X-ray diffraction (XRD, Miniflex 600, Cu K $\alpha$  radiation,  $\lambda = 1.5418 \text{ \AA}$ ). The morphology of the MOF, the surface and cross-section of the separator, and the elemental mapping of the MOF were characterized by scanning electron microscope (TESCAN VEDA3) and field emission scanning

electron microscope (FEI Nova Nano SEM 450). Thermogravimetric analysis (TGA) curves were obtained with a thermal analyzer (STA 449F3). The functional groups of the carbonized MOFs were measured by Fourier transform infrared spectroscope (FTIR, Tensor 27). The degree of graphitization for the carbonized MOFs was characterized by Raman spectroscope (Raman, LabRAM HR). The state of the carbonized MOF was characterized by X-ray photoelectron spectroscope (XPS, Thermo Scientific PHI 5000). The pore distribution of the MOF after carbonization was measured by nitrogen adsorption and desorption (BET, ASAP 2460).

### 2.5. Electrochemical performance test

The CR2016 coin cell battery was assembled in an argon-filled glove box. Lithium metal was used as the anode, 1,2-dimethoxyethane (DME) and 1,3-dioxolane (1:1 volume ratio), 1 mol·L<sup>-1</sup> lithium bis(trifluoromethanesulfonyl)imide and a mixture of 0.2 mol·L<sup>-1</sup> LiNO<sub>3</sub> were used as the electrolyte. Cycling and rate performance tests were performed on a battery tester (LAND, CT-3001 A) at room temperature in the voltage range of 1.8–2.8 V. Furthermore, cyclic voltammetric (CV) test was performed at a scan rate of 0.1 mV·s<sup>-1</sup> and on a multi-channel electrochemical workstation (PGSTAT302N) with a voltage range of 1.8–2.8 V, and electrochemical impedance spectroscopic (EIS) measurements were made in the frequency range of 100 kHz to 10 mHz.

## 3. Results and discussion

The Ni-MOF, Co-MOF, and (Ni,Co)-MOF prepared by liquid-phase stirring method were yellow-green, purple, and pink, respectively, as black powders (Fig. S1). The carbonized MOF was easily adhered to the weighing paper, indicating that the dispersibility of the material was improved. As shown in Fig. 1a–c, at a magnification of 9 K, the uncarbonized MOF exhibits a columnar structure with a smooth surface. Affected by poor conductivity, streaks appear on SEM images. The Ni-MOF, Co-MOF and (Ni,Co)-MOF cylinders are approximately 0.6  $\mu\text{m}$  in diameter, and 7, 11 and 8  $\mu\text{m}$  in length, respectively. As the cobalt content increases, the length of the MOF becomes longer. The (Ni,Co)-MOF has both long and short cylinders, giving it the advantage of point-to-surface bonding. As shown in Fig. 1d–f, the carbonized Ni/C is easy to agglomerate, but Co/C has good dispersibility, and (Ni,Co)/C has both characteristics, which is conducive to the combination of long-range and short-range. To further analyze the surface topography of the carbonized MOFs,

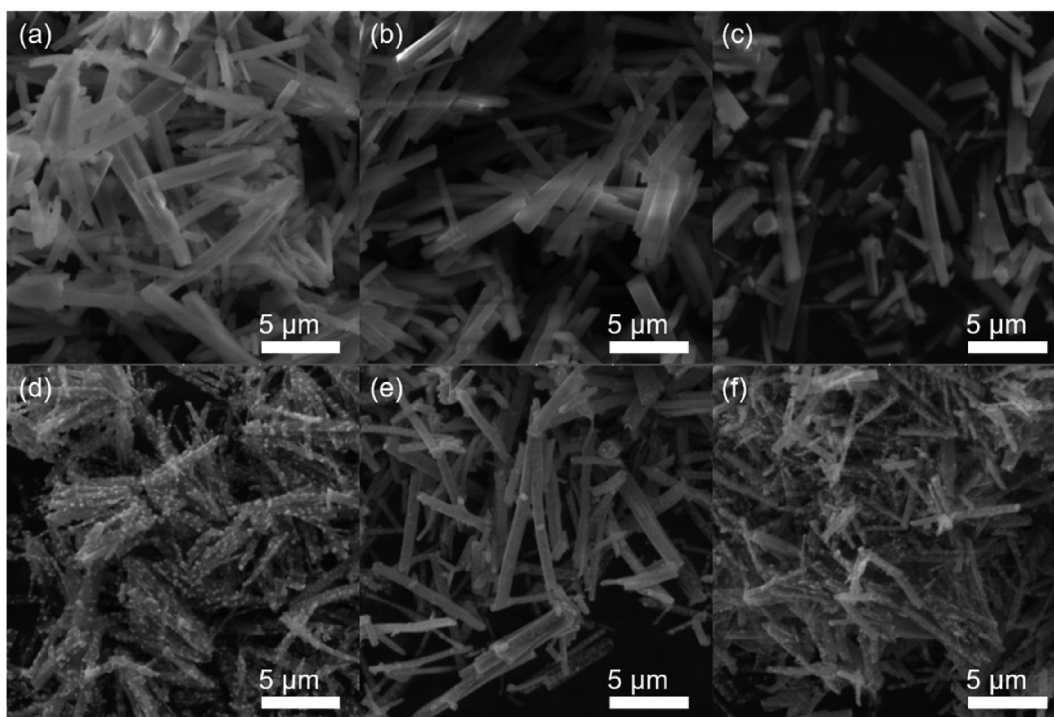


Fig. 1. SEM images of Ni-MOF(a), Co-MOF(b), (Ni,Co)-MOF(c), Ni/C(d), Co/C(e) and (Ni,Co)/C(f).

field emission SEM analysis was performed on Ni/C, Co/C, and (Ni,Co)/C (Fig. 2). After the MOF was carbonized, metal element particles appeared on the surface. The aggregated particles on the Ni/C surface are larger, while the aggregated particles on the Co/C surface are smaller, with a large number of aggregates inside. The metal particles are uniformly distributed inside and on the surface of (Ni,Co)/C. It can be seen that (Ni,Co)/C not only can suppress a large amount of metal agglomeration, but also can avoid the material agglomeration. The catalytic activity of transition metals on the surface of MOF-derived carbons and the internal porous structure can be used for sulfur fixation. By analyzing the types and contents of (Ni,Co)/C surface elements, it can be seen that oxygen and transition metal elements are uniformly distributed on the surface of the columnar carbon material, indicating that the transition metal elements are uniformly distributed. Its surface functional groups are evenly distributed. Surface scanning elemental analysis shows (Fig. 3) that the approximate content ratios of Ni and Co were similar, consistent with the ICP results (Table S1). The content of nickel ions in Ni-MOF was 21%, while the content of cobalt ions in Co-MOF was 22%, and the contents of nickel ions and cobalt ions in (Ni,Co)-MOF were 11% and 11.7%, respectively, the nickel-cobalt ratio in (Ni,Co)-MOF was 0.94. The metal ion content is basically the same as the original design. No loss

of metal elements occurred during the process. This result shows that the preparation method in this paper overcomes the current problem that binary metals are difficult to react synchronously with organic ligands.

In order to explore the crystal structure changes of MOF before and after carbonizations, XRD tests were carried out. As shown in Fig. 4, the diffraction peaks of Co-MOF and (Ni,Co)-MOF have certain similarity, indicating that the two crystal forms are similar. The Ni/C, Co/C and (Ni,Co)/C all have carbon peaks at  $26^\circ$ , indicating that the carbon composite layer was formed *in situ* after carbonization at high temperature. The diffraction peaks of Ni/C at  $44^\circ$ ,  $52^\circ$  and  $76^\circ$  correspond to the (111), (200) and (220) crystal planes of elemental nickel, respectively, and the diffraction peaks of Co/C at  $44^\circ$ ,  $52^\circ$  and  $76^\circ$  correspond to the (111), (200) and (220) crystal planes of elemental cobalt, while the diffraction peaks of Ni at  $44^\circ$ ,  $52^\circ$ , and Co/C at  $76^\circ$  correspond to the (111), (200) of elemental nickel, and the (220) crystal plane of cobalt. There are no impurity peaks in the three, and the carbide crystallinity is relatively high. Since cobalt and nickel have the same main group and the same period, thus they have similar physical and chemical properties. The binary metals can easily participate in the reaction in the preparation process, and are uniformly dispersed in the MOF structure, so that the (Ni,Co)-MOF is uniformly crystallized.

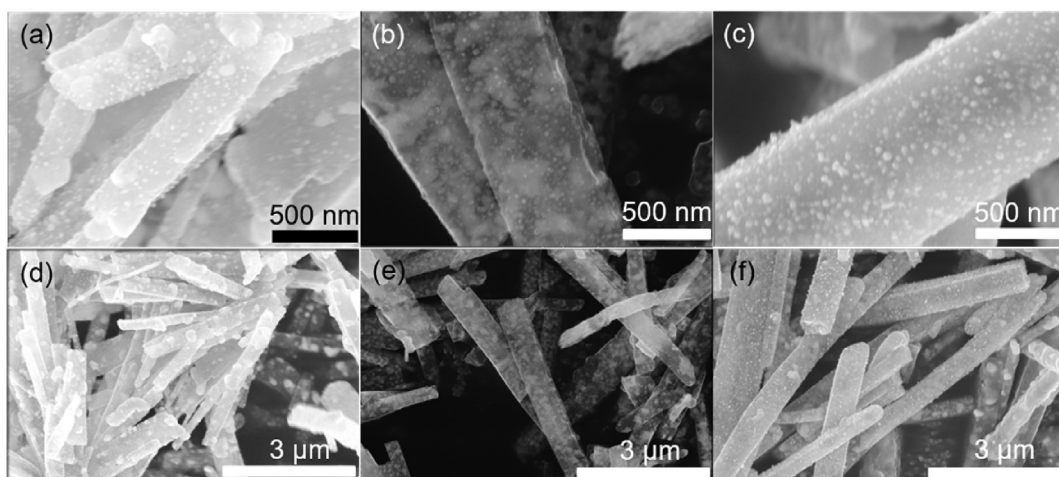


Fig. 2. FESEM images of Ni/C (a, d), Co/C (b, e) and (Ni,Co)/C (c, f).

Thermogravimetric tests were carried out for the as-prepared MOF materials under argon atmosphere. Fig. S2 shows the TG-DSC curves of Ni-MOF, Co-MOF and (Ni, Co)-MOF. The changes of the three curves are roughly the same and can be divided into three stages, followed by dehydration, pyrolysis and carbonization [22]. A dehydration reaction occurred at 35–210 °C to remove gas and water molecules adsorbed on the surface. It can be seen that the weight loss rate of Ni-MOF in the first stage (about 20%) was relatively obvious. This is because that the nickel metal element easily absorbs moisture. However, due to the special element distribution and material structure, the Co-MOF only reduced the weight by 12%. With the increase of temperature, the organic ligands on the surface of MOF began to be decomposed by heat to generate gases such as oxygen, hydrogen, carbon dioxide and carbon monoxide. The weight loss rate in the second stage was related to the

complexation of organic ligands. The weight loss rates of the three MOF materials at this stage are similar, indicating that they have similar complexing abilities with organic ligands. The carbonization reaction started in the third stage, and the carbon element in the organic ligands in the previous stage began to undergo graphitization reaction, and the transition metal ions were reduced to elemental metals (Equations (1) and (2)). Monometallic MOFs exist in elemental form, while the exist form of bimetal-MOF requires further study. The carbonization reaction has an exothermic peak at about 900 °C, which may be caused by the exothermic reaction of material crystallization. All three MOFs are in the exothermic peak range at this temperature. Therefore, choosing 900 °C as the carbonization temperature is beneficial to increase the graphitization of the carbon layer, and the crystallinities of Ni and Co.

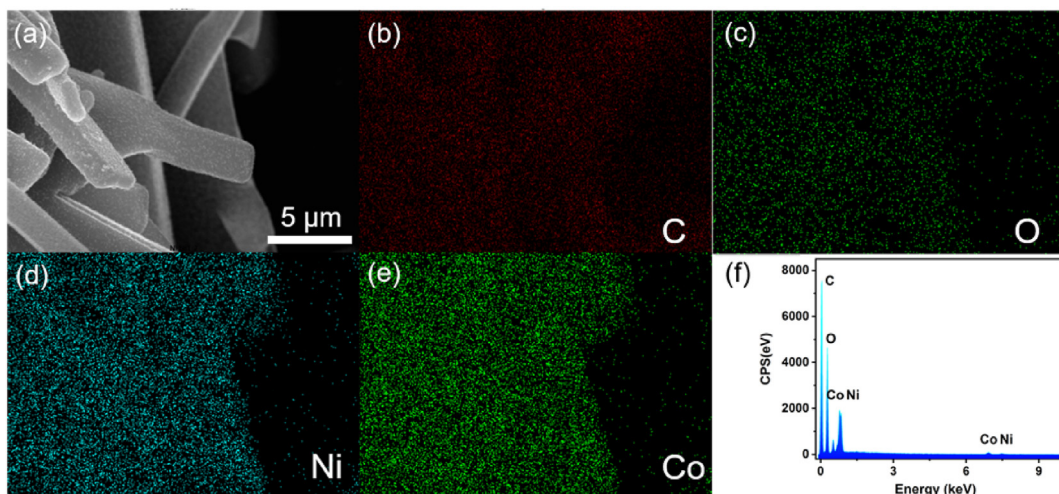


Fig. 3. EDS images of (Ni,Co)/C.

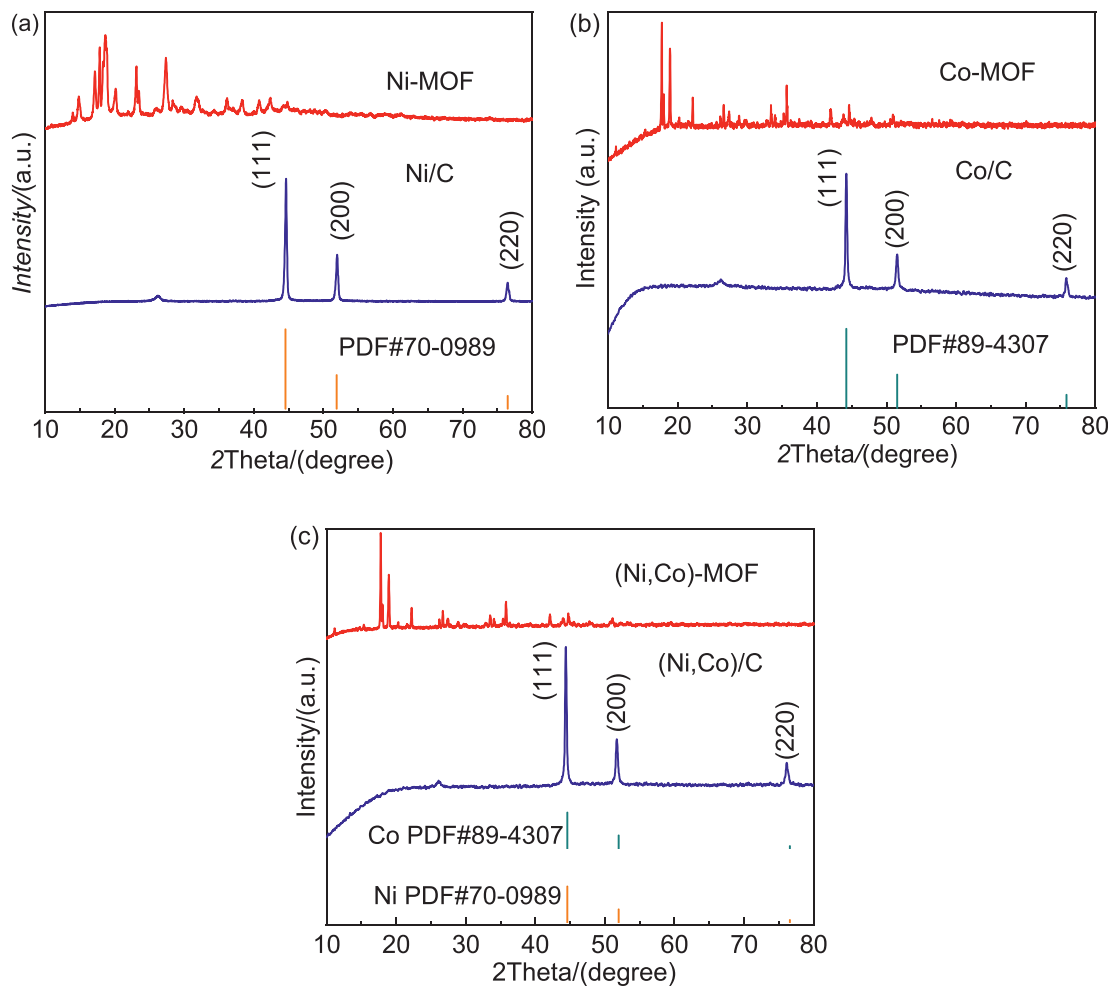


Fig. 4. XRD patterns of Ni/C(a), Co/C(b) and (Ni,Co)/C(c).



Fig. 5a is the Raman spectra of Ni/C, Co/C and (Ni,Co)/C. The G and D bands located at ca. 1594 and 1352  $\text{cm}^{-1}$  represent the crystalline graphite band and the defect-induced band,

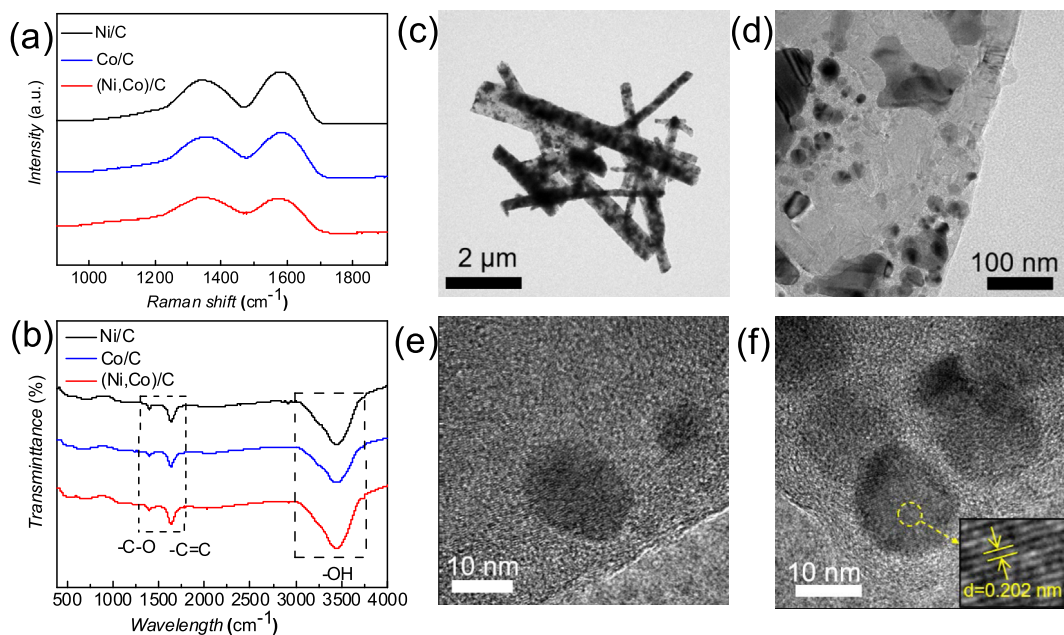


Fig. 5. Raman (a) and FTIR (b) spectra of Ni/C, Co/C and (Ni,Co)/C. HRTEM image of (Ni,Co)/C (c). XPS curves of Ni/C(d), Co/C(e) and (Ni,Co)/C (f).

respectively. The intensity ratios ( $I_D/I_G$ ) of Ni/C, Co/C and (Ni,Co)/C were 0.88, 0.93 and 1.02, respectively. Among them, (Ni,Co)/C has the highest degree of graphitization [23,24], the existence of a large number of defects provides catalytic active sites for the electrochemical reaction in LSB, and the fine grains are beneficial to shorten the transport distance of lithium ion, thereby increasing the transmission rate. The absorption peaks at 1396, 1642 and 3428  $\text{cm}^{-1}$  in Fig. 5b represent the vibrational absorptions of  $-\text{CO}$  bond,  $-\text{C}=\text{C}$  bond and  $-\text{OH}$  bond, respectively, indicating that MOF acting as the precursors can

generate oxygen-containing functional groups [18,25].

The high-resolution transmission electron microscopic image (Fig. 5c) shows that (Ni,Co)/C is in the shape of columns of different lengths, proving that it can have long- and short-range combined conduction. The black particles on the surface are simple transition metals composed of heavy elements, while the transparent part is a carbon layer composed of light elements, and the metal particles are uniformly distributed inside and on the surface of the carbon layer. At a magnification of 20 K (Fig. 5d), it can be observed

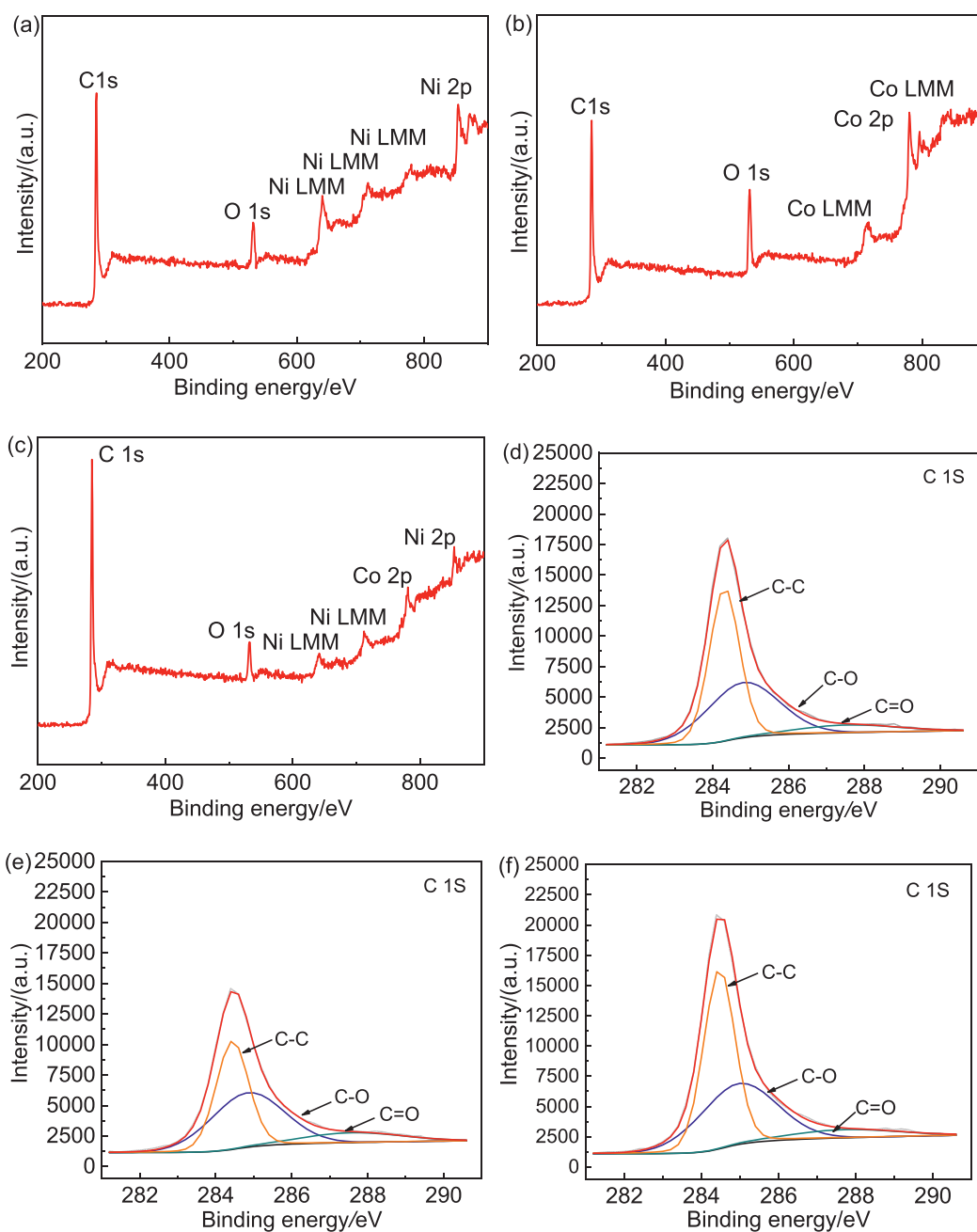


Fig. 6. C 1s XPS spectra of Ni/C (a), Co/C (b) and (Ni,Co)/C (c). BET curves of Ni/C (d), Co/C (e) and (Ni,Co)/C (f).

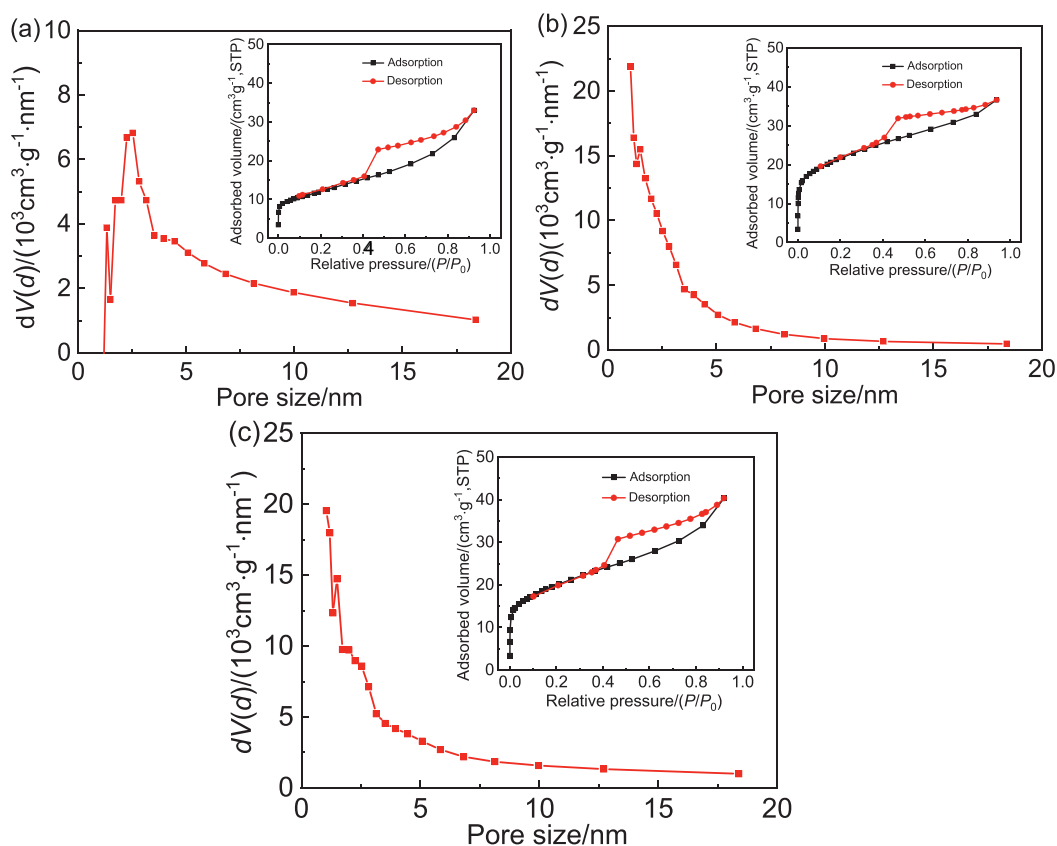


Fig. 7. BET curves of Ni/C (a), Co/C (b) and (Ni,Co)/C (c).

that the size of the metal particles on the surface of the carbon layer is 6 nm. Analysis of the lattice fringes (Fig. 5e and f) shows the uniform and smooth lattice. The stripes correspond to the (111) plane of Ni or Co, and the interplanar spacing is about 0.202 nm. In addition, the diffraction ring has no lattice diffraction spots, which proves that (Ni,Co)/C is an amorphous carbon material.

The element type and chemical bond composition of the MOF-derived materials were known by XPS analysis. Fig. 6a–c are the total spectra of XPS. Due to the complexation of trimesic acid, Ni/C, Co/C and (Ni,Co)/C all contain carbon and oxygen in addition to their respective metal elements, achieving the effect of self-doping oxygen. The (Ni,Co)/C had the highest carbon content, which indicates that the synergistic effect of the bimetals contributes to the enhanced carbon content of the MOF. The sub-peak fitting of C 1s is shown in Fig. 6d–f, three sub-peaks can be obtained for Ni/C, Co/C and (Ni,Co)/C, and C–C, C–O, C=O in Ni/C are calculated by integral fitting. The molar ratios of C–O were 50.91%, 41.21% and 7.88%, respectively. The molar ratios of C–C, C–O, and C=O in Co/C were 42.95%, 45.8% and 11.25%, respectively. The molar ratios of C=O were 51.91%, 40.41% and 7.69%, respectively, indicating that the carbon

layer of the MOF after carbonization has abundant C–O and C=O.

The Ni/C, Co/C and (Ni,Co)/C were all type IV isotherms from the nitrogen adsorption and desorption curves of MOF-derived metal/carbon composites (Fig. 7), indicating that all three are mesoporous materials. There are H4-type hysteresis loops, and the pore structure is usually slit pores, which are composed of a mixture of micropores and mesopores to form a multi-layered pore structure, similar to activated carbon, which is beneficial to adjust the surface properties of carbon materials. The specific surface areas of Ni/C, Co/C and (Ni,Co)/C were calculated to be 62.6, 99.4 and 96.1  $\text{m}^2 \cdot \text{g}^{-1}$ , respectively, from the BJH structure.

The planar and cross-sectional morphologies of the Ni/C, Co/C and (Ni,Co)/C modified separators were observed by SEM and are shown in Fig. 8. Fig. 8a–c are plan views of Ni/C modified separator, Co/C modified separator and (Ni,Co)/C modified separator. It can be seen that columnar carbon is scattered on the surface of the separator, Ni/C and (Ni,Co)/C are in the shape of thinner rods, while Co/C is in the shape of thicker rods. Co/C is uniformly dispersed on the PE surface, while Ni/C is not uniformly dispersed, and the

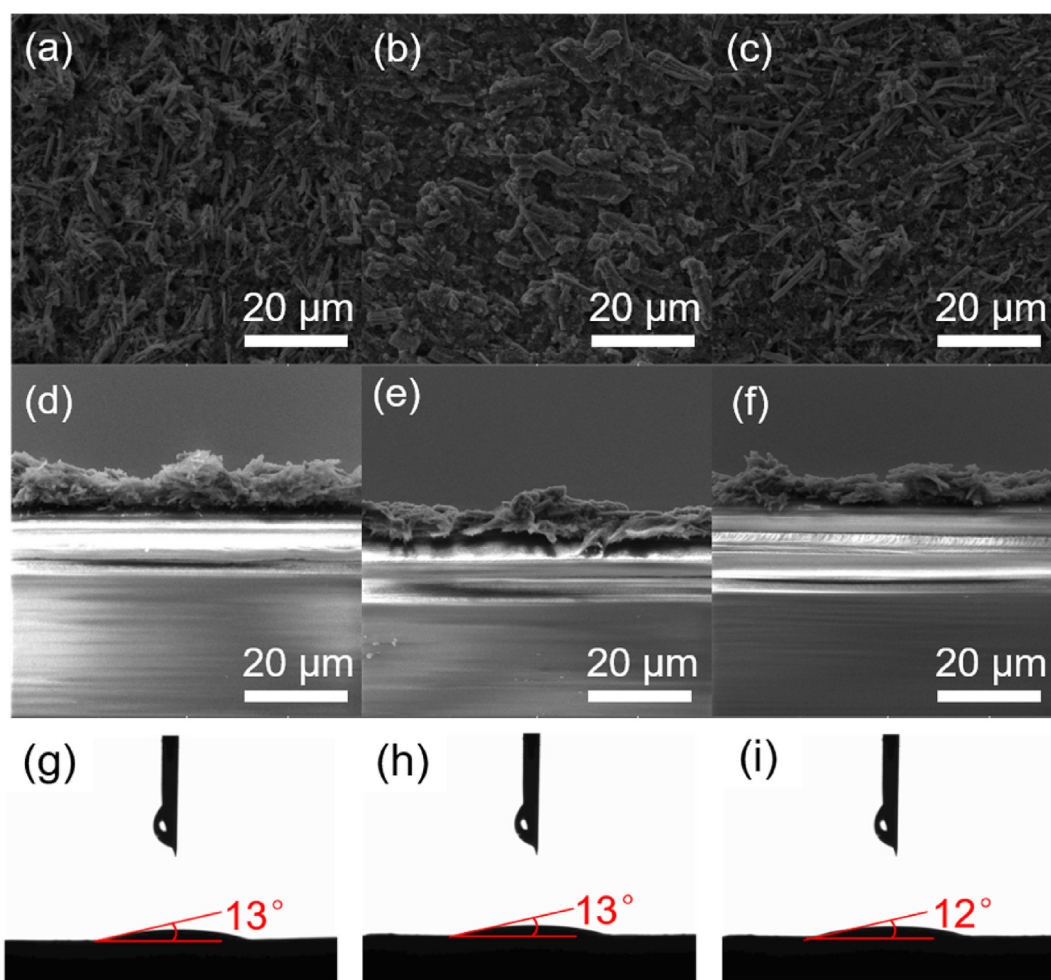


Fig. 8. SEM images of Ni/C modified (a), Co/C modified (b), and (Ni,Co)/C modified (c) separators. Cross-sectional SEM images of Ni/C modified (d), Co/C modified (e) and (Ni,Co)/C modified (f) separators. Electrolyte contact-angle tests of Ni/C modified (g), Co/C modified (h), and (Ni,Co)/C modified (i) separators.

whole is in a dense state. (Ni,Co)/C is in a point-to-surface bonding state, which is beneficial to improve the tap density on the surface of the separator, and provides various forms of channels for different carriers, so that the charge density distribution is uniform, thereby reducing the concentration polarization. As shown in Fig. 8d–f, by measuring the thickness of the membrane modified layer, it was found that due to the presence of agglomerations, the thickness of Ni/C was uneven. In contrast, the (Ni, Co)/C combined with long and short columns was more uniform, which was more conducive to improving the lithium ion transport efficiency and improving the electrochemical reaction rate of the battery.

As shown in Fig. 8g–i, the LSB electrolyte was dropped on the modified separator, the smaller the contact angle between the electrolyte and the separator at the same time, the better the wettability of the modified layer to the electrolyte. The wetting angles of Ni/C modified separator, Co/C

modified separator and (Ni,Co)/C modified separator were 13°, 13° and 12°, respectively. Compared with the unmodified PE separator (Fig. S3), the wettability of the electrolyte with Ni/C, Co/C and (Ni,Co)/C modified separators is improved owing to the modification of the separator. The abundant polar functional groups on the surface of the layer play a role.

Thermal stability test is an important research method to measure the safety of the battery. The modified separator was placed in an oven at 160 °C for 30 min and taken out, and then photos before and after heating were taken. The results are shown in Fig. 9. It can be seen from the thermal stability test that the PE has changed from the original white round shape to a transparent oval shape, and even dents appear on the surface, and the area shrinkage rate is as high as 20%. The area shrinkage rates of Ni/C modified separator, Co/C modified separator and (Ni,Co)/C modified separator were only 15.1%, 15.8% and 15.3%,

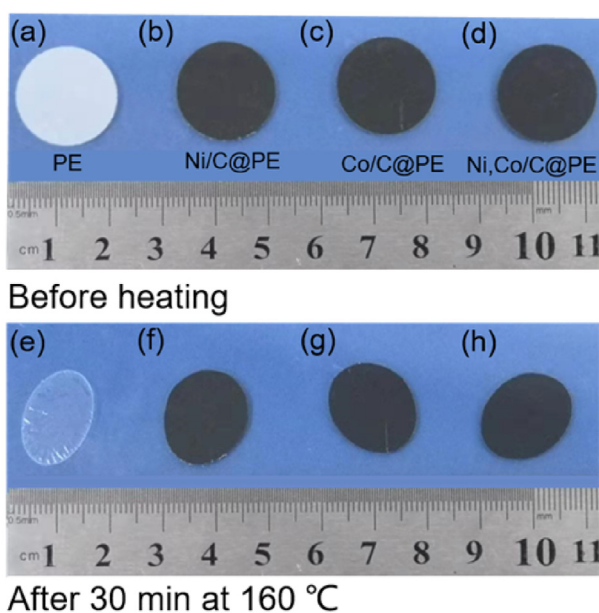


Fig. 9. Photographs showing the thermal stabilities of PE separator (a, e), Ni/C modified separator (b, f), Co/C modified separator (c, g) and (Ni, Co)/C modified separator (d, h).

respectively, which are much lower than that of PE. After the separator is modified by MOF carbon material, its thermal shrinkage deformation is suppressed to a certain extent.

The MOF-derived carbon-modified separator assembled cells were tested by cyclic voltammetry, as shown in Fig. 10a–c. After four cycles, the cyclic voltammetric curves of the (Ni,Co)/C modified separator have the highest coincidence degree, which proves that the (Ni,Co)/C modified separator battery has good cycling stability. The two reduction peaks during the discharge are located at 2.05 V and 2.35 V. During the charging process, the sulfur cathode undergoes an oxidation reaction, and the oxidation peaks are located at 2.3 V and 2.4 V. The oxidation peaks of Ni/C modified separator, Co/C modified separator and (Ni,Co)/C modified separator all appears sub-peaks, but at different potentials. The oxidation reaction of LSB consists of two steps. Since the reaction rates of S4 generation and S4 consumption in common sulfur cathodes are the same, the rates of charge transfer and ion diffusion are similar, the reaction can proceed rapidly, so the oxidation peak is in the form of a single peak. The transition metals in Ni/C, Co/C and (Ni,Co)/C act as catalysts for electrochemical reactions, reducing the energy barrier of the oxidation reaction and shifting the peak positions to the low potential region. The polarization voltages of Ni/C, Co/C and (Ni,Co)/C decrease sequentially, indicating that the synergistic effect of bimetals can effectively accelerate the electrochemical reaction rate.

In the charge-discharge curves of LSB with different modified separators, two typical discharge plateaus corresponding to the “solid-liquid-solid” transition of LIPS can be clearly observed (Fig. 10d–f). From the perspective of capacity contribution (Fig. 11a), the first platform on Ni/C accounts for a larger proportion, indicating that its catalytic effect is better from long chains than short chains. In order to study the change of battery specific capacity under different current densities, rate performance tests were carried out. The first cycle discharge specific capacity of the (Ni,Co)/C modified separator was as high as  $1238.1 \text{ mAh}\cdot\text{g}^{-1}$ , and the initial Coulombic efficiency was 98.7%. The specific discharge capacities of Ni/C modified separator and Co/C modified separator were  $1138.9$  and  $1099.6 \text{ mAh}\cdot\text{g}^{-1}$ , respectively. The excellent first-turn capacity is mainly due to the improved utilization of polysulfide active materials by the modified layer of the separator. Among them, due to the synergistic effect of nickel-cobalt binary metal, the improvement effect of (Ni,Co)/C modified separator is more obvious. With the increase of cycle number, the overlapping degree of the three charge-discharge curves is higher, indicating that the cycle stability of the battery is higher. The charging curve has two voltage plateaus, which are consistent with the cyclic voltammetric results. The plateau voltages of the three discharge processes are stable at 2.3 V and 2.1 V under different cycles. The voltage plateau of the charging process was 2.3–2.4 V, but the difference among the three is obvious, mainly because the nickel-cobalt binary metal accelerates the kinetic process of the polysulfur reaction and affects the thermodynamic process of the solvent interface. Fig. 11b is the cycle performance graph at 0.2 C. After 100 cycles, the battery with (Ni,Co)/C still maintained a capacity of  $861.8 \text{ mAh}\cdot\text{g}^{-1}$ , showing excellent cycling stability.

In order to study the change of battery specific capacity under different current densities, rate performance tests were carried out. As shown in Fig. 11c, the (Ni,Co)/C modified separator exhibited a reversible discharge capacity of  $1389.9 \text{ mAh}\cdot\text{g}^{-1}$  at 0.1 C. When the current density was increased to 0.2 C, 0.5 C, 1 C, 2 C, and 5 C, the reversible discharge specific capacities were  $1235.9$ ,  $1094.9$ ,  $927.7$ ,  $728.2$ , and  $556.9 \text{ mAh}\cdot\text{g}^{-1}$ , respectively. When the current density was restored to 0.1 C, its reversible discharge capacity was  $1237.5 \text{ mAh}\cdot\text{g}^{-1}$ , which could reach 89% of the initial value. The specific capacities of Ni/C and Co/C modified separators were  $522.5 \text{ mAh}\cdot\text{g}^{-1}$  and  $401.5 \text{ mAh}\cdot\text{g}^{-1}$  at 5 C, respectively. When the current

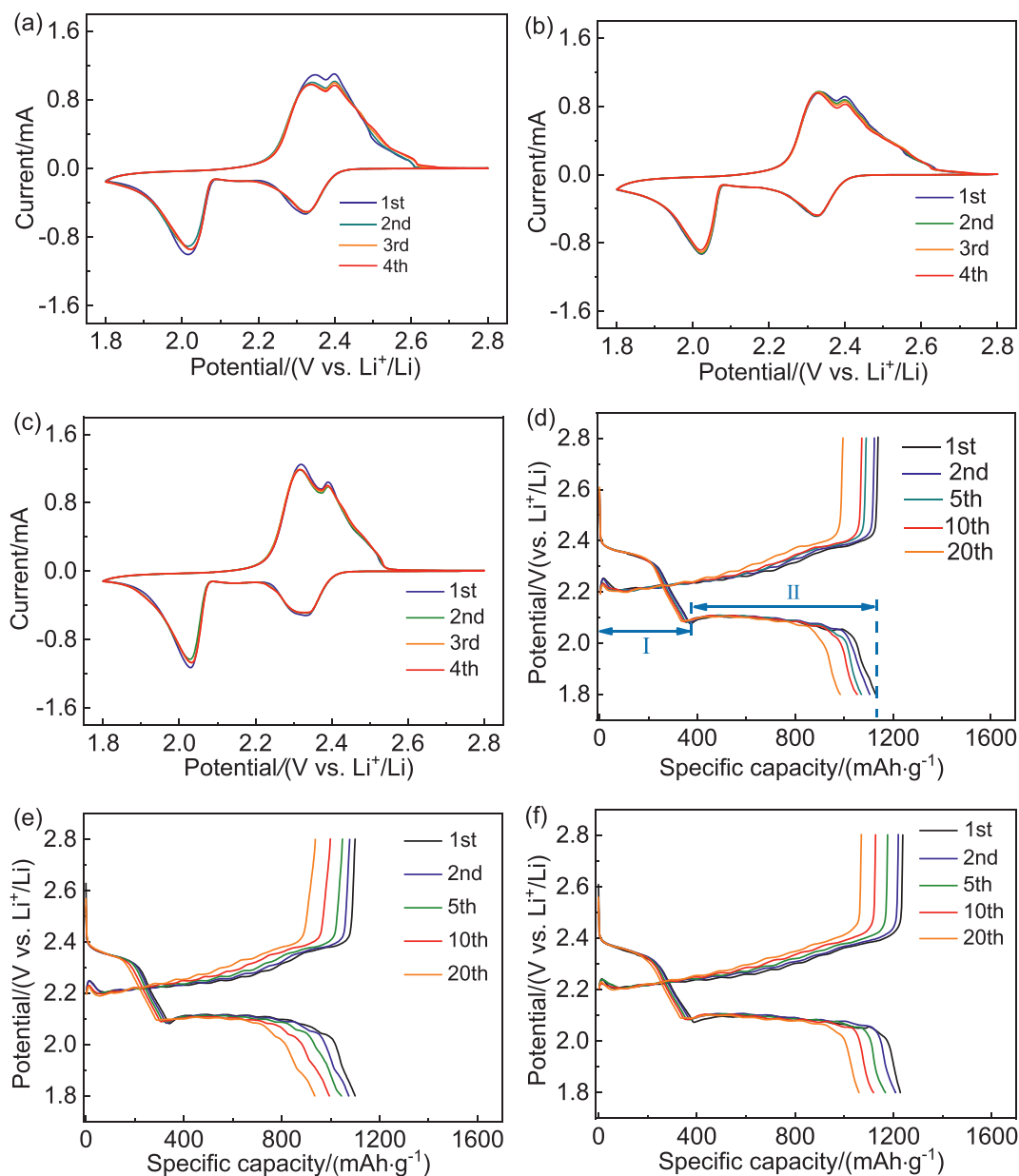


Fig. 10. Cyclic voltammograms of LSB with Ni/C (a), Co/C (b), and (Ni,Co)/C (c) modified separators. The charge-discharge curves of LSB with Ni/C (d), Co/C (e), and (Ni,Co)/C (f) modified separators at different cycles.

density was restored to 0.1 C, the capacities were 1121.3 and 1060.5  $\text{mAh}\cdot\text{g}^{-1}$ , respectively, which were 85% and 82.2% of the initial values, respectively. The nickel-cobalt binary metal accelerates the electrochemical kinetics, making the (Ni,Co)/C modified separator have the most excellent rate performance.

Long-cycle charge-discharge tests were performed at high current densities. The cycling performance of Ni/C, Co/C and (Ni,Co)/C modified separators at 1 C current density for 500 cycles is shown in Fig. 11d. The first cycle discharge specific capacity of the (Ni,Co)/C modified separator was

as high as  $1035.6 \text{ mAh}\cdot\text{g}^{-1}$ . The first cycle discharge capacities of Ni/C and Co/C modified separators were  $964.7$  and  $897.9 \text{ mAh}\cdot\text{g}^{-1}$ , respectively, which are lower than that of (Ni, Co)/C modified separator. When the number of cycles reached 500, the reversible capacity of the (Ni,Co)/C modified separator was  $662.2 \text{ mAh}\cdot\text{g}^{-1}$  with the capacity retention rate of 63.9%. At this time, the reversible capacities of the Ni/C and the Co/C modified separators were  $602.2$  and  $593 \text{ mAh}\cdot\text{g}^{-1}$ , respectively. The capacity retention rates were lower than that of the (Ni,Co)/C modified separator. This reflects the excellent reaction stability and structural

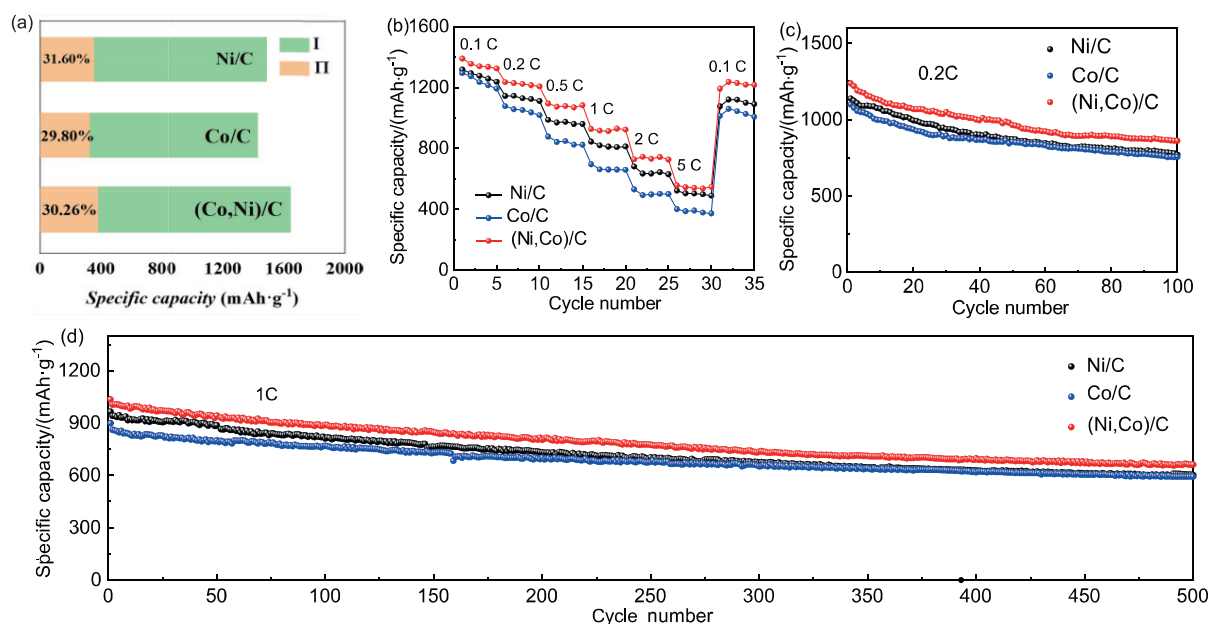


Fig. 11. Capacity contribution diagram of LSB with Ni/C, Co/C and (Ni,Co)/C modified separators (a). Cycling performance of LSB with Ni/C, Co/C and (Ni,Co)/C modified separators at 0.2 C current density (b). Rate capability of LSB with Ni/C, Co/C and (Ni,Co)/C modified separators (c). Cycling performance of LSB with Ni/C, Co/C and (Ni,Co)/C modified separators at 1 C current density (d).

stability of the modified separator system, which is mainly due to the abundant porous carbon materials that optimize the electrical conductivity of polysulfides and transition metal-catalyzed electrochemical reactions.

The color experiment can verify the effect of the separator on inhibiting the shuttle of polysulfide ions. As shown in Fig. 12a–f, the separator was placed between a solution containing  $1 \text{ mmol} \cdot \text{L}^{-1} \text{Li}_2\text{S}_6$  and a solution without  $1 \text{ mmol} \cdot \text{L}^{-1} \text{Li}_2\text{S}_6$ . The solvent for the two passes was DME: DOL (1:1). After standing for 12 h, in the Ni/C modified separator and Co/C modified separator samples,  $\text{Li}_2\text{S}_6$  gradually diffused to the solvent side driven by the concentration potential energy, and the liquid on the left gradually changed from colorless to yellow. The color of the solution on the left side of the (Ni,Co)/C modified separator sample hardly changed. It is shown that the (Ni,Co)/C modified separator can effectively inhibit the shuttle of polysulfide ions.

In order to study the effect of the modified separator on the reaction kinetics and conductivity of lithium ions in LSB, the lithium ion migration number and ion diffusion coefficient of the modified separator battery were tested. Symmetric cells were assembled with spacers/spacers, and their EIS values were tested by AC impedance, and the results are shown in Fig. S4. The  $\sigma$  values of the Ni/C, Co/C and (Ni,Co)/C modified separators were 1.184, 1.03 and  $2.369 \text{ mS} \cdot \text{cm}^{-1}$ , respectively

(Equation S(1)). Compared with the ordinary separator ( $0.78 \text{ mS} \cdot \text{cm}^{-1}$ ), the electrical conductivity of the modified separator is improved, and the conductivity of the (Ni,Co)/C modified separator is the most obvious. The combination of long-range and short-range conductivity of the (Ni,Co)/C modified separator modified layer improves the conductivity of lithium ions, which is beneficial to the transport of lithium ions in the electrode, and reduces the polarization of the electrochemical cell system, as well as optimizes its large electrochemical performance under current. The conductivity of polysulfides is further improved, and the utilization rate of sulfur active materials and the reversible capacity of the battery are also improved.

The lithium ion migration number is a factor that determines the effect of the separator on the electrochemical performance of the battery. The charge transfer undertaken by lithium ions reflects the charge-discharge characteristics of the battery, so increasing the number of lithium ions' migration is beneficial to improve the conductivity of the electrolyte. Potentiostat amperometric test was performed in a lithium/lithium symmetric cell before and after the tests, as shown in Fig. 12g. The lithium ion migration numbers of the Ni/C, Co/C and (Ni,Co)/C modified separators were 0.603, 0.5065 and 0.698, respectively (Equation S(2)). The MOF carbon composite modified separator improves the lithium ion migration number, and the

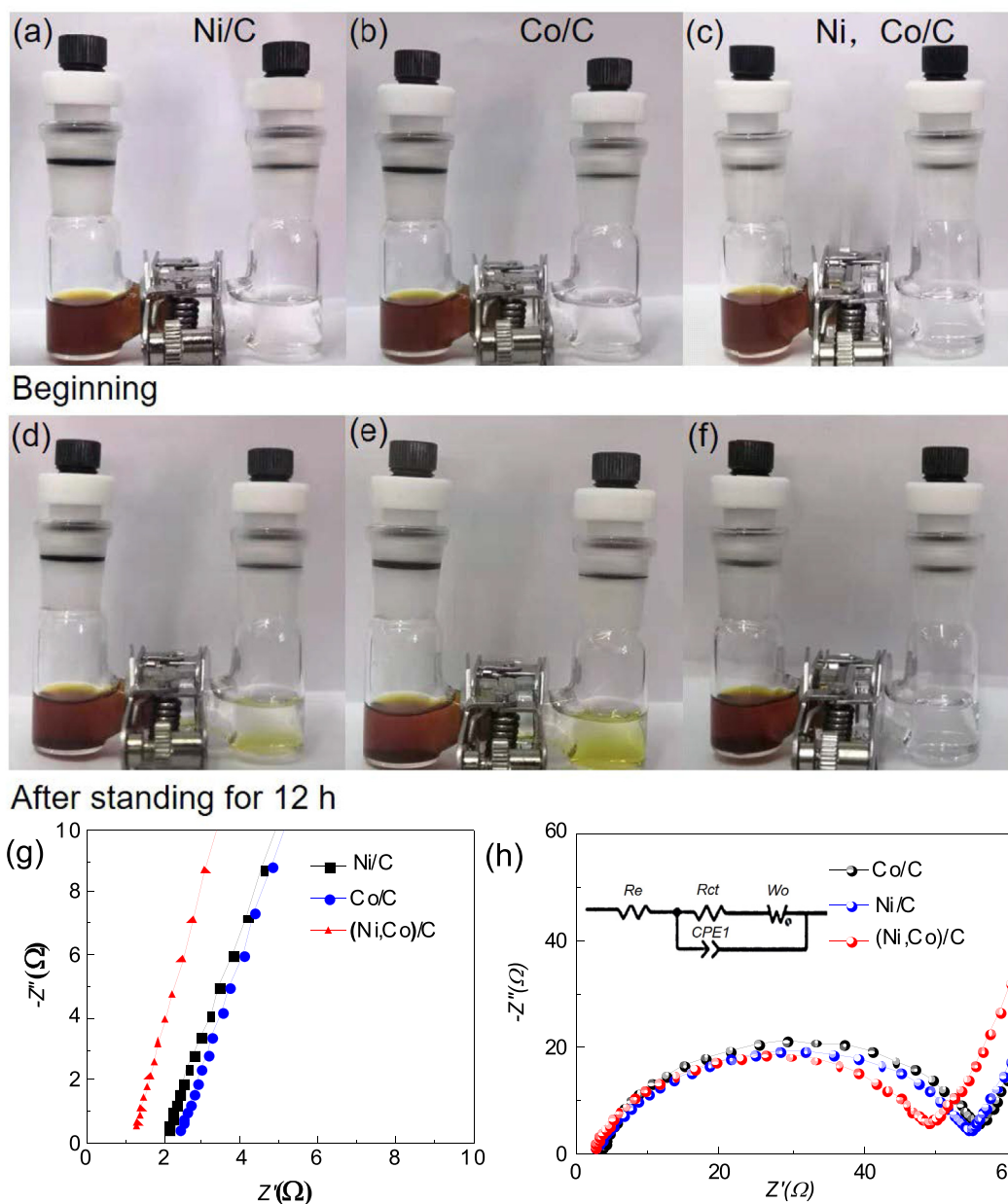


Fig. 12. Polysulfide ion shuttle experiments of Ni/C (a, d), Co/C (b, e) and (Ni, Co)/C (c, f) modified separators. Ion diffusivity (g) and Nyquist (h) plots of Ni/C, Co/C and (Ni,Co)/C modified separators (the inset in (h) is the equivalent circuit diagram).

(Ni,Co)/C modified separator has the best improvement effect. This is mainly due to the interaction between the porous structure of the composite carbon layer and the transition metal bonds, which accelerates the migration of lithium ions and improves the rate performance of the battery, which is consistent with the rate performance test results.

In order to analyze the reaction resistance and diffusion mass transfer process parameters of the battery charge transfer process, the AC impedance test was carried out. The semicircle reflects the charge transfer resistance ( $R_{ct}$ ) of the sulfur electrode and the high frequency intercept on the real

axis represents the resistance ( $R_e$ ) of the electrolyte. The AC impedance curves of Ni/C, Co/C and (Ni,Co)/C modified separators are shown in Fig. 12h. Among the three modified separators, the (Ni,Co)/C modified separator has the smallest impedance, which proves that the (Ni,Co)/C modified separator has the best charge transfer ability and smaller interfacial impedance.

#### 4. Conclusions

This work overcomes the difficulty in the preparation of bimetal-MOFs, and uses a simple and rapid room temperature liquid phase synthesis

method to prepare columnar nickel-cobalt bimetal-MOFs [(Ni,Co)-MOFs]. The (Ni,Co)/C obtained by high-temperature carbonization was used to modify the LSB separator to alleviate the shuttle effect of polysulfides and accelerate the conversion kinetics between polysulfides. The results demonstrated that the (Ni,Co)/C modified layer ensures fast ion transport across the separator and effectively traps polysulfides, while promoting the kinetics of long-chain sulfur to short-chain sulfur conversion. The first-cycle discharge specific capacity of LSB was  $1238.1 \text{ mAh}\cdot\text{g}^{-1}$  at 0.2 C rate and  $1035.6 \text{ mAh}\cdot\text{g}^{-1}$  at 1 C rate. The (Ni,Co)/C@PE battery could still maintain a specific capacity of  $979 \text{ mAh}\cdot\text{g}^{-1}$  after 100 cycles at 0.2 C. The rate performance of the (Ni,Co)/C@PE battery had also been significantly improved. As the current density increased to 0.2 C, 0.5 C, 1 C, 2 C and 5 C, the reversible discharge specific capacity could reach 1235.9, 1094.9, 927.7, 728.2 and  $556.9 \text{ mAh}\cdot\text{g}^{-1}$ , respectively.

## Acknowledgements

This work was supported by Yunnan Fundamental Research Projects (Grant NO. 202001AU070079, 202101BE070001-018, 202101AT070214, 202101AW070006), and Yunnan ZhongYan Industry Co., Ltd. Science and Technology Project (2020GY03).

## References

- [1] Wei Z Z, Zhang N X, Wu F, Chen R J. Progress and prospects on multifunctional coating separators for lithium-sulfur battery[J]. *J. Electrochem.*, 2020, 26(5): 716–730.
- [2] Lin J X, Qu X M, Wu X H, Peng J, Zhou S Y, Li J T, Zhou Y, Mo Y X, Ding M J, Huang L, Sun S G. NiCo<sub>2</sub>O<sub>4</sub>/CNF separator modifiers for trapping and catalyzing polysulfides for high-performance lithium-sulfur batteries with high sulfur loadings and lean electrolytes[J]. *ACS Sustainable Chem. Eng.*, 2021, 9(4): 1804–1813.
- [3] Wu F, Ye Y S, Chen R J, Qian J, Zhao T, Li L, Li W H. Systematic effect for an ultralong cycle lithium-sulfur battery [J]. *Nano Lett.*, 2015, 15(11): 7431–7439.
- [4] Wu F, Qian J, Chen R J, Ye Y S, Sun Z G, Xing Y, Li L. Light-weight functional layer on a separator as a polysulfide immobilizer to enhance cycling stability for lithium-sulfur batteries[J]. *J. Mater. Chem.*, 2016, 4(43): 17033–17041.
- [5] Ye Z Q, Jiang Y, Feng T, Wang Z H, Li L, Wu F, Chen R J. Curbing polysulfide shuttling by synergistic engineering layer composed of supported Sn<sub>4</sub>P<sub>3</sub> nanodots electrocatalyst in lithium-sulfur batteries[J]. *Nano Energy*, 2020, 70: 104532.
- [6] Wei L, Li W L, Zhao T, Zhang N X, Li L, Wu F, Chen R J. Cobalt nanoparticles shielded in N-doped carbon nanotubes for high areal capacity Li-S batteries[J]. *Chem. Commun.*, 2020, 56(20): 3007–3010.
- [7] Yao W Q, Tian C X, Yang C, Xu J, Meng Y F, Manke J, Chen N, Wu Z L, Zhan L, Wang Y L, Chen R J. P-doped NiTe<sub>2</sub> with Te-vacancies in lithium-sulfur batteries prevents shuttling and promotes polysulfide conversion[J]. *Adv. Mater.*, 2022, 34(11): 2106370.
- [8] Li Z, Zhang F, Cao T, Tang L B, Xu Q J, Liu H M, Wang Y G. Highly stable lithium-sulfur batteries achieved by a SnS/porous carbon nanosheet architecture modified celgard separator[J]. *Adv. Funct. Mater.*, 2020, 30(48): 2006297.
- [9] Zuo Y Z, Zhu Y J, Tang X S, Zhao M, Ren P J, Su W M, Tang Y F, Chen Y F. MnO<sub>2</sub> supported on acrylic cloth as functional separator for high-performance lithium-sulfur batteries[J]. *J. Power Sources*, 2020, 464: 228181.
- [10] Kim S, Lim W G, Cho A, Jeong J, Jo C, Kang D G, Han S M, Han J W, Lee J. Simultaneous suppression of shuttle effect and Li dendrite growth by light-weight bifunctional separator for Li-S batteries[J]. *ACS Appl. Energy Mater.*, 2020, 3(3): 2643–2652.
- [11] Li W L, Qian J, Zhao T, Ye Y S, Xing Y, Huang Y X, Wei L, Zhang N X, Chen N, Li L, Wu F, Chen R J. Boosting high-rate Li-S Batteries by an MOF-derived catalytic electrode with a layer-by-layer structure[J]. *Adv. Sci.*, 2019, 6(16): 1802362.
- [12] Ye Z Q, Jiang Y, Li L, Wu F, Chen R J. Enhanced catalytic conversion of polysulfide using 1D CoTe and 2D MXene for heat-resistant and lean-electrolyte Li-S batteries[J]. *Chem. Eng. J.*, 2022, 430: 132734.
- [13] Liu Y T, Liu S, Li G R, Gao X P. Strategy of enhancing the volumetric energy density for lithium-sulfur batteries[J]. *Adv. Mater.*, 2021, 8(33): 2003955.
- [14] Mikhaylik Y V, Akridge J R. Polysulfide shuttle study in the Li/S battery system[J]. *J. Electrochem. Soc.*, 2004, 151(11): A1969–A1976.
- [15] Xuan W M, Zhu C F, Liu Y, Cui Y. Mesoporous metal-organic framework materials[J]. *Chem. Soc. Rev.*, 2012, 41(5): 1677–1695.
- [16] Zheng J M, Tian J, Wu D X, Gu M, Xu W, Wang C M, Gao F, Engelhard M H, Zhang J G, Liu J, Xiao J. Lewis acid-base interactions between polysulfides and metal organic framework in lithium sulfur batteries[J]. *Nano Lett.*, 2014, 14(5): 2345–2352.
- [17] Sun L, Campbell M G, Dinca M. Electrically conductive porous metal-organic frameworks[J]. *Angew. Chem., Int. Ed.*, 2016, 55(11): 3566–3579.
- [18] Zang Y, Pei F, Huang J H, Fu Z H, Xu G, Fang X L. Large-area preparation of crack-free crystalline microporous conductive membrane to upgrade high energy lithium-sulfur batteries[J]. *Adv. Energy Mater.*, 2018, 8(31): 1802052.
- [19] Qi C, Xu L, Wang J, Li H L, Zhao C C, Wang L N, Liu T X. Titanium-containing metal-organic framework modified separator for advanced lithium-sulfur batteries[J]. *ACS Sustain. Chem. Eng.*, 2020, 8(34): 12968–12975.
- [20] Li W L, Ye Y S, Qian J, Xing Y, Qu W, Zhang N X, Li L, Wu F, Chen R J. Oxygenated nitrogen-doped microporous nanocarbon as a permselective interlayer for ultrastable lithium-sulfur batteries[J]. *Chemelectrochem*, 2019, 6(4): 1094–1100.
- [21] Zhang Z, Wang J N, Shao A H, Xiong D G, Liu J W, Lao C Y, Xi K, Lu S Y, Jiang Q, Yu J, Li H L, Yang Z Y, Kumar R V. Recyclable cobalt-molybdenum bimetallic carbide modified separator boosts the polysulfide adsorption-catalysis of lithium sulfur battery[J]. *Sci. China Mater.*, 2020, 63(12): 2443–2455.
- [22] Bauer I, Thieme S, Brueckner J, Althues H, Kaskel S. Reduced polysulfide shuttle in lithium-sulfur batteries using Nacion-based separators[J]. *J. Power Sources*, 2014, 251: 417–422.
- [23] Zhou J W, Li R, Fan X X, Chen Y F, Han R D, Li W, Zheng J, Wang B, Li X G. Rational design of a metal-organic

- framework host for sulfur storage in fast, long-cycle Li-S batteries[J]. *Energy Environ. Sci.*, 2014, 7(8): 2715–2724.
- [24] Xu Y X, Zheng S S, Tang H F, Guo X T, Xue H G, Pang H. Prussian blue and its derivatives as electrode materials for electrochemical energy storage[J]. *Energy Storage Mater.*, 2017, 9: 11–30.
- [25] Wu X, Fan L S, Qiu Y, Wang M X, Cheng J H, Guan B, Guo Z K, Zhang N Q, Sun K N. Ion-selective prussian-blue-modified celgard separator for high-performance lithium-sulfur battery[J]. *ChemSusChem*, 2018, 11(18): 3345–3351.

## CoNi 基双金属-有机骨架衍生碳复合材料多功能改性锂硫电池隔膜

王妍洁<sup>a,#</sup>, 程宏宇<sup>a,#</sup>, 侯冀岳<sup>a</sup>, 杨文豪<sup>a</sup>, 黄荣威<sup>a</sup>, 倪志聪<sup>a</sup>, 朱子翼<sup>a</sup>, 王颖<sup>a,b</sup>, 韦克毅<sup>c</sup>, 张义永<sup>a,\*</sup>, 李雪<sup>a,\*</sup>

<sup>a</sup> 昆明理工大学冶金与能源工程学院, 锂离子电池与材料制备技术国家地方联合工程实验室, 云南省先进电池材料重点实验室, 云南 昆明 650093

<sup>b</sup> 攀枝花大学智能制造学院, 四川 攀枝花 617000

<sup>c</sup> 云南中研实业有限公司技术中心, 云南 昆明 650231

### 摘要

严重的多硫化物穿梭效应和转化缓慢等问题导致锂硫电池容量迅速衰减, 其大规模应用受限。本文将金属有机框架材料 (MOF) 衍生碳(Ni,Co)/C 用于锂硫电池隔膜改性, 很好地解决了上述问题。钴镍双金属的协同作用分别实现了大量又快速的化学固硫和抑硫的可逆性, 显著提高了锂硫电池的循环稳定性和倍率性能。在 1 C 的电流密度下, (Ni,Co)/C 改性隔膜电池的容量在第 1 次循环时可以达到 1035.6 mAh·g<sup>-1</sup>, 在 500 次循环后容量仍保持 662.2 mAh·g<sup>-1</sup>, 容量保持率为 63.9%。此外, 本工作克服了二元金属基 MOF 制备难的问题, 使用简单快速的室温液相合成法制备了柱状镍钴二元 MOF, 该法有望实现 MOF 的宏观制备。

**关键词:** 锂硫电池; 隔膜改性; 双金属有机框架; 穿梭效应